

**Key Points:**

- Cyclone landfall angle plays an important role in modulating storm surge along the New Jersey coastline
- The degree of sensitivity to landfall angle varies along the coastline, pointing to the importance of landfall location
- Storms with tracks perpendicular to the coast produced the highest storm surge levels and the broadest offshore extent and inland flooding

Supporting Information:

- Supporting Information Data S1

Correspondence to:

A. N. Ramos-Valle,
alexandra.ramos@rutgers.edu

Citation:

Ramos-Valle, A. N., Curchitser, E. N., & Bruyère, C. L. (2020). Impact of tropical cyclone landfall angle on storm surge along the Mid-Atlantic Bight. *Journal of Geophysical Research: Atmospheres*, 125, e2019JD031796. <https://doi.org/10.1029/2019JD031796>

Received 11 OCT 2019

Accepted 24 JAN 2020

Accepted article online 29 JAN 2020

Impact of Tropical Cyclone Landfall Angle on Storm Surge Along the Mid-Atlantic Bight

Alexandra N. Ramos-Valle¹ , Enrique N. Curchitser¹ , and Cindy L. Bruyère^{2,3}

¹Department of Environmental Sciences, Rutgers University, New Brunswick, NJ, USA, ²National Center for Atmospheric Research, Boulder, CO, USA, ³Environmental Sciences and Management, North-West University, Potchefstroom, South Africa

Abstract Storm surge impact depends on coastal geographical and bathymetric features as well as various tropical cyclone characteristics including the size, intensity, and impact angle of the storm. Although the factors contributing to storm surge are well studied, uncertainties remain regarding the level of sensitivity to these parameters. This work seeks to contribute to the current knowledge of storm surge by studying the sensitivity to tropical cyclone landfall angle. We perform an ensemble of synthetic tropical cyclones using a newly developed modeling capability derived from the Weather Research and Forecasting (WRF) model, the Hybrid WRF Cyclone Model. Wind and atmospheric pressure field outputs from 200 synthetic cyclones are used as atmospheric forcing for the Advance Circulation (ADCIRC) model. We study the sensitivity of storm surge offshore extent and inundation to tropical cyclone impact angle. The extent of the impact area around the landfall location is sensitive to the cyclone landfall angle. Cyclones with tracks perpendicular to the coast are shown to produce the highest water levels and broadest inland and offshore extent. Results also indicate a heterogeneity in the sensitivity to landfall angle along the coast, highlighting the importance of both cyclone impact angle and location.

Plain Language Summary Storm surge is often the most devastating threat resulting from tropical cyclones. The magnitude of storm surge impact depends on features of the coastline and the characteristics of the cyclones including the intensity, size, and the angle at which the storms approach the coastline. Slight changes in any of these factors can change the expected impact location and severity of the storm surge event. However, uncertainties remain in understanding the degree to which storm surge varies in response to changes in the characteristics of the storms. In this work, we seek to understand how changes in the cyclone impact angle along the New Jersey coast affect the storm surge magnitude, extent, and location. We use a new modeling capability that allows us to simulate cyclones that are physically plausible but that have not been observed in the past, and their resulting storm surge. Results from this study suggest that there is in fact a dependency of storm surge to landfall impact angle along the New Jersey coastline. Depending on the storm landfall angle, the impact area broadens around the landfall point. Results highlight different responses along the coast pointing to the importance of cyclone impact angle and location.

1. Introduction

Tropical cyclones (TCs) represent the most destructive atmospheric events in the United States (Smith & Katz, 2013). Often, the resulting TC-induced storm surge has more of a destructive impact than have precipitation and winds alone. The potential damages due to storm surge depends on local geographic and bathymetric features, as well as on TC characteristics such as intensity, size, speed, and angle of landfall with respect to the coast. The lack of accurate meteorological observations prior to landfall makes the understanding, assessment, and prediction of storm surge challenging. Previous hindcast storm surge modeling studies (Dietrich, Westerink, et al., 2011; Dietrich, Zijlema, et al., 2011; FEMA, 2011; FEMA, 2014b; Mayo & Lin, 2019) have provided accounts of errors from the hydrodynamic models typically used such as the Sea, Lake and Overland Surges from Hurricanes (SLOSH) model (Jelesnianski et al., 1992) and the Advanced Circulation (ADCIRC) model (Luettich et al., 1992; Luettich & Westerink, 2004). Mayo and Lin (2019) found that on average the SLOSH model, used by the National Weather Service for operational storm surge forecasting, tends to underestimate peak storm surge levels by 22%. For the case of Hurricane Gustav,

Dietrich, Westerink, et al. (2011) used ADCIRC and found an overall error of 0.14 m. For the New Jersey-New York (NJ-NY) region, average ADCIRC model peak storm surge error is found to be 0.32 m (FEMA, 2011, 2014b).

An added complicating factor in assessing storm surge impacts is the limited North Atlantic TC and water elevation record. A recent review on TC-induced storm surge accounts for availability of water level data for 110 cases along the entire U.S. Atlantic Coast since 1880 (Needham et al., 2015). Only 22% of the 110 events occurred along the coastline from Virginia to Maine (Needham et al., 2015). Despite their relatively infrequent occurrence along the northern portion of the U.S. Atlantic Coast, these surge events have produced substantial damages. In particular, the NJ-NY region is characterized by these low-frequency and high-impact TC- and extratropical (Booth et al., 2016; Colle et al., 2008; Lin et al., 2019; Needham et al., 2015) cyclone-induced storm surge events. Most notable are the Long Island Express Hurricane (1983), which produced storm surge of 3.0–3.5 m in Long Island (Lin et al., 2010), and more recently Hurricane Sandy (2012), a transitioning extratropical cyclone that tested the resilience of the NJ-NY coastal region with typical storm surge heights of about 3–4 m (Blake et al., 2013).

The vulnerability of such regions highlights the need for improved understanding of the underlying processes contributing to storm surge impacts. Atmospheric forcing is a primary driver of storm surge, and it represents one of the main sources of uncertainty in storm surge modeling (Gonzalez et al., 2019; Kohno et al., 2018; Lin & Chavas, 2012; Mayo & Lin, 2019). Therefore, determining the sensitivity of storm surge to different TC physical parameters is an important step in increasing forecasting accuracy. Previous studies examined the impact on storm surge from changes in TC intensity (Weisberg & Zheng, 2006), size (Irish et al., 2008), forward speed (Hussain et al., 2017; Rego & Li, 2009; Thomas et al., 2019; Weisberg & Zheng, 2006), and location (Fossell et al., 2017; Galarneau et al., 2013). The relationship between storm surge and some of the storm parameters are more straightforward to determine, but others such as the effect of storm translational speed and angle of landfall on storm surge have proven to be more complicated and difficult to assess.

Historically, the behavior observed along the NJ region, and more broadly along the eastern United States, is for cyclones to move northward along the coast (Hall & Sobel, 2013). However, Hurricane Sandy was an example of the possibility of storms impacting land from other directions. While various factors contributed to its record-breaking storm surge, part of the impact is attributed to its rare near-perpendicular angle of landfall (Hall & Sobel, 2013). As such, Hurricane Sandy put into perspective the need to determine storm surge sensitivity to storm track and landfall angle in the NJ-NY coastal region. The impact of changing a TC's landfall angle on storm surge has not been studied in as much detail as other cyclone parameters. Moreover, studies specific to the NJ-NY region are lacking in this respect. In this study, we seek to address the uncertainty in the impact of TC landfall angle on storm surge in the NJ-NY coastal region.

The model specifications, coupling details and a summary of the simulations performed are provided in section 2. Results from the atmospheric and storm surge ensembles are presented in section 3, and their implications are discussed in section 4. Finally, a summary and conclusions from the study are available in section 5.

2. Materials and Methods

Simulations of synthetic cyclones were performed with the Hybrid Weather Research and Forecasting (WRF) Cyclone Model (HWCM) and used as meteorological forcing for the Simulating Waves Nearshore (SWAN; Booij et al., 1999) and ADCIRC (SWAN+ADCIRC; Dietrich, Zijlema, et al., 2011) coupled surge-wave model (Ramos-Valle, 2019). A case study of three synthetic cyclones with different landfall angles was conducted to examine the impact of approach angle on storm surge. The case study was expanded to include the analysis of a large number of synthetic cyclones along the NJ coastline. The synthetic cyclones were grouped into three categories, as given by the general direction of their tracks. The average storm surge produced by these scenarios was analyzed, and vulnerable coastal locations were identified. Finally, a clustering algorithm was performed on the storm surge model simulations for a more detailed assessment of the factors influencing the different storm surge responses. In the following section, the model techniques used for the work presented are described.

2.1. HWCM Configuration

Simulations of TCs were conducted with the HWCM; an extension of the WRF (Skamarock et al., 2008) model that enables the simulation of synthetic cyclones in a real-world domain. Bruyère et al. (2019) provide an in-depth description and evaluation of the HWCM model setup. Here an overview of the model and its configuration to simulate synthetic TCs is provided. The simulation process was split into two steps as the HWCM makes use of both the real and idealized components of WRF (for details on the configuration of idealized cyclones in WRF, see Rotunno et al., 2009). To set up the HWCM simulations, a cyclone was spun up in an idealized configuration. This cyclone was then placed in a real-world domain where it could dynamically develop and propagate.

To achieve the first step, a weak initial vortex was placed within an idealized atmosphere, which was defined as the 10-year average September climatology for the Western North Atlantic region bounded within latitudes 33°N and 41°N and longitudes –70.0°W and –75.5°W. The initial atmospheric conditions were spatially constant throughout the simulation domain. The atmospheric vertical profile was constructed with data from the National Centers for Environmental Prediction/National Center for Atmospheric Research Reanalysis 1 (Kalnay et al., 1996). Low-level instabilities in the vertical profile (Figure 1) were smoothed out to ensure that the resulting environment was supportive of cyclone formation and development. In practice, the background environment can be provided by any profile-based data set. Using a 10-year September climatological mean ensures a realistic environment able to sustain TC development throughout the length of the simulation.

The initial vortex was set up to represent a TC-like axisymmetric vortex with tropical depression strength (maximum wind speed of 15 m/s), outer radius of 412.5 km and radius of maximum winds of 150 km, based on the vortex derived by Rotunno and Emanuel (1987). The extent of the radius of maximum winds was increased from the default value of 82.5 km to account for larger cyclones. The simulation uses a spatially constant Coriolis parameter of $5.0 \times 10^{-5} \text{ s}^{-1}$, corresponding to 20°N. The TC was positioned in the center of the domain and spun up for a period of 12 days in the idealized domain with constant sea surface temperatures (SSTs) of 28°C. The horizontal resolution was set to 12 km. No lateral boundary conditions were needed for this step as periodic boundaries were used.

Once a mature TC was established in the idealized plane, the first step in the simulation process was completed. As a second step, the cyclone was then placed in a real-world domain. As described by Bruyère et al. (2019), the real-world domain is characterized as a β -plane with real coastlines and topography. The real-world domain contained all the characteristics inherent to real simulations in WRF such as prescribed land mask, terrain height, land use type, and albedo.

As in typical real-case simulations, the TC was allowed to dynamically evolve in response to the imposed atmospheric and sea surface conditions. The initial environmental conditions were similar to those used in the idealized configuration. Additionally, in the real-world simulations, the background wind flow was prescribed and set up to provide a constant flow at the boundaries. The HWCM allows for adjustment of the placement of the TC in the real-world domain and of the speed and direction of the background wind flow. The ability to vary these properties allow for a degree of control of the TC landfall location, angle of landfall, and TC translation speed, while still permitting the TC to dynamically evolve, propagate, and interact with the surrounding environment and topography (Bruyère et al., 2019).

Four-day simulations of synthetic TCs were performed using the real simulation capabilities of the WRF model v3.8. The simulations were performed on a 12-km horizontal resolution grid (same as in the idealized simulation) and ran with 38 vertical levels and model top at 50 mb. The horizontal resolution used, while somewhat coarser than suggested to accurately capture TC intensity (Lakshmi et al., 2017; Mori et al., 2014), was chosen to balance the need for sufficient accuracy with our ability to simulate a large number of cyclones (Bruyère et al., 2019). The physical parameterizations implemented were previously tested on a similar domain and model configuration for the case of Hurricane Sandy (Ramos-Valle et al., 2018) and were used by the National Center for Atmospheric Research for hurricane simulations for domains of comparable horizontal resolution to that of 12 km used in this study (Galarneau et al., 2013). The parameterization schemes used include the following: WRF single-moment 6-class microphysics scheme (Hong & Lim, 2006), Yonsei University boundary layer scheme (Hong et al., 2006), Tiedtke cumulus parameterization (Tiedtke, 1989), Rapid Radiative Transfer Model for General Circulation Models for shortwave and

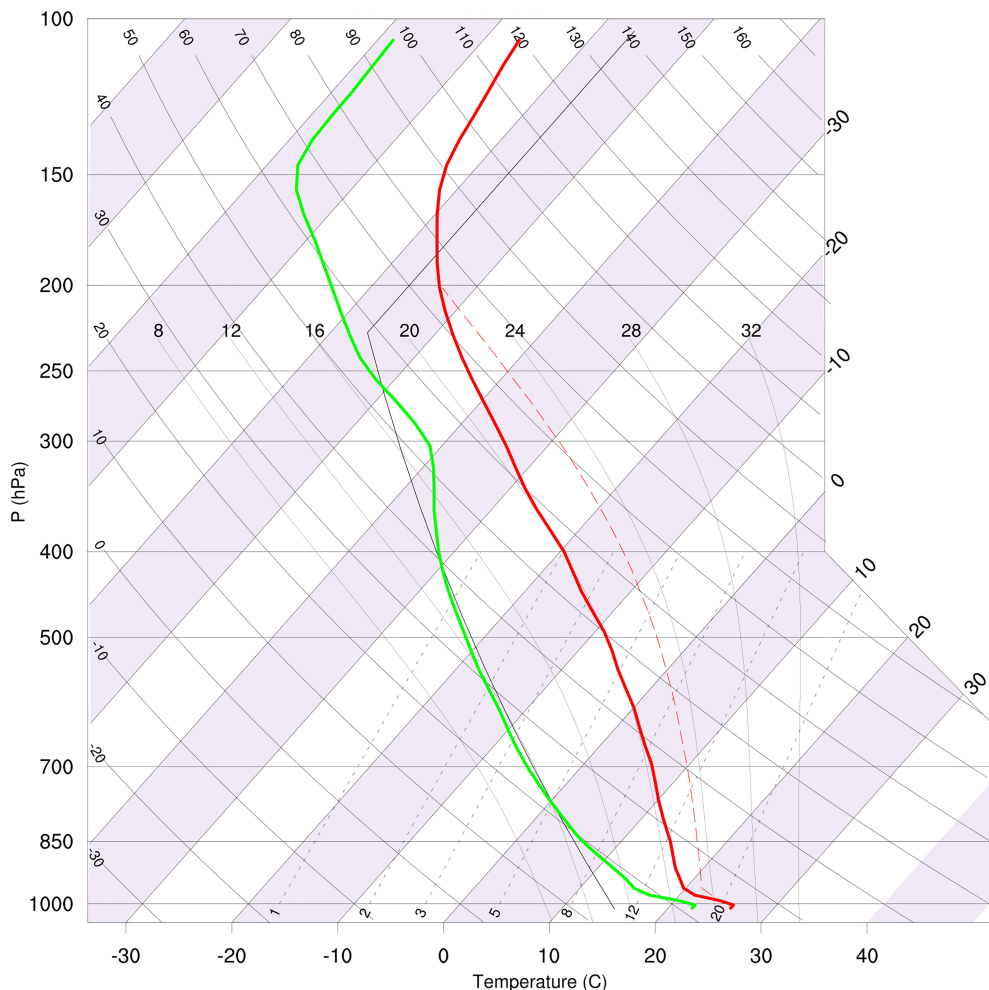


Figure 1. Atmospheric vertical profile used to characterize the environment in the ideal and real simulations. Values were interpolated to account for missing data at various pressure levels. The atmospheric temperature and dew point are shown in the red and green lines, respectively.

longwave radiation parameterization (Iacono et al., 2008), and the Noah land surface model (Chen & Dudhia, 2001). The SST remained time invariant and spatially uniform at 28 °C (Bruyère et al., 2019; Kimball, 2008; Li et al., 2015). As reported by Bruyère et al. (2019), a constant SST does not negatively impact the development of cyclones, and on the contrary, its effect is that of sustaining a stronger TC throughout the simulation. The choice of a constant SST adds the benefit for less complexity by simplifying the differences between the simulated TCs and allowing for a more direct comparison between simulations. Since a cyclone was effectively transposed from one environment to another, a 2-hr digital filter initialization (Peckham et al., 2016) scheme was implemented to reduce initial model instabilities and allow the simulations additional spin-up time.

Alternative approaches are available to simulate synthetic cyclones for storm surge applications, including the use of parametric vortex models (e.g., Dynamic Holland Model; Holland, 1980) and statistical-deterministic TC models (Emanuel et al., 2006; Lin et al., 2012). Track-based data are implemented within parametric models, which allows for easy manipulation of storm characteristics to study the individual impact of storm parameters. Various studies have compared the use of parametric models with more realistic wind field representations (Akbar et al., 2017; Bennett & Mulligan, 2017; Ramos-Valle et al., 2018; Torres et al., 2018), including the use of the WRF model. Full physics atmospheric models have proven to be more accurate, albeit at a larger computational cost (Ramos-Valle et al., 2018). The use of the HWCM ensures fidelity in generating physically plausible storms that dynamically interact and respond to their surroundings,

Table 1*Description of Parameters Chosen to Initialize the Real-World Simulations*

Initial TC category	Initial TC intensity (m/s)	Initial TC location	Background wind speed (m/s)
Category 2	46	Point A: 38.7358, -68.8555	8
Category 3	54	Point B: 36.5861, -69.5870	10
Category 4	61	Point C: 34.9458, -73.5707	12

with more accurate wind field representations. Not only does the HWCM present the advantage of allowing a high degree of control over cyclone parameters, but it also allows for sensitivity studies of climate change (by variation of SST or other environmental factors). The methodology is applicable to other regions, facilitating sensitivity studies in other areas. We present the first application of the HWCM for storm surge assessment.

2.2. Description of Synthetic Cyclone Simulations With the HWCM

The HWCM allows flexibility in adjusting various parameters when placing a TC in the real-world domain. By solely changing the speed and direction of the background steering flow, as well as the initial location of the TC in the real-world domain, a range of possible evolution scenarios for the same initial TC can be simulated. In this study, three different initial cyclones with intensities representative of Category 2, 3, and 4 storms were examined. For each case, one of three parameters were varied at a time: the initial location of the TC in the real-world domain, the speed of the background wind flow, and the direction of the wind flow (Table 1).

Three points were selected as initial locations for the placement of the TCs. The locations of these points were chosen to allow for coverage of a large portion of the domain in order to simulate probable TC tracks. While the average tracks of North Atlantic TCs are often north-northeastward (Hall & Sobel, 2013), the choice of the initial cyclone location in this study promotes the simulation of cyclones from various directions and landfall impact angle that may not be observed in the historical records but nevertheless are physically plausible. It is important to highlight that these points do not represent cyclogenesis locations, as the TCs were fully developed by the time they were placed at each point in the real-world domain. Additionally, the speed of the background wind flow was chosen to vary between 8, 10, and 12 m/s. All directional wind angles in 45° intervals were tested. The directional angle frequency was increased by 5° intervals within the bounds that produced landfalling TCs. Since the focus of the study is primarily on storms that have a direct impact on the coast, only the TCs that made landfall along the NJ-NY coastline were considered. This method produced between 2 and 12 tracks for each of the 27 configurations.

2.3. SWAN+ADCIRC Model Description and Atmospheric Forcing Configuration

Coastal impacts from the synthetic storms were assessed by using the two-dimensional depth integrated (2DDI) implementation of the ADCIRC hydrodynamic model (Luettich et al., 1992; Luettich & Westerink, 2004), coupled with the SWAN wave model (SWAN+ADCIRC). The SWAN model includes processes such as wave growth due to wind and action loss due to white capping, surf breaking, and bottom friction.

ADCIRC has been implemented for various coastal studies in the region of interest along the NJ-NY coastal area (Cialone et al., 2017; Colle et al., 2015; Lin et al., 2010; Ramos-Valle et al., 2018; Yin et al., 2016). The ADCIRC model uses a finite-element unstructured triangular grid allowing for higher resolution near the coast and coarser resolution in the deep ocean. The ADCIRC mesh is made up of elements, each of which contains three nodes or vertices where water heights are computed. In this study, simulations were performed on a grid developed by the Federal Emergency Management Agency (FEMA) as part of the Region II Coastal Storm Surge Study (FEMA, 2014a). Various studies have validated and implemented the use of this mesh to study TCs and extratropical cyclones (Orton et al., 2015; Ramos-Valle et al., 2018; Yin et al., 2016). The mesh domain contains a total of 604,790 nodes and includes the U.S. Atlantic Coast, the Gulf of Mexico, and the Caribbean. Increased resolution is found in areas including the Delaware Bay, the Hudson River Valley, New York City, and Long Island Sound (LIS) (Figure 2). The mesh inland extent was constructed based on the 25-ft NAVD88 contour (FEMA, 2014a), resulting in a broader inland extent in southern NJ and a narrower extent in northern NJ. The inland extent of the mesh (Figure 2) can be interpreted as the potential or maximum inundation area.

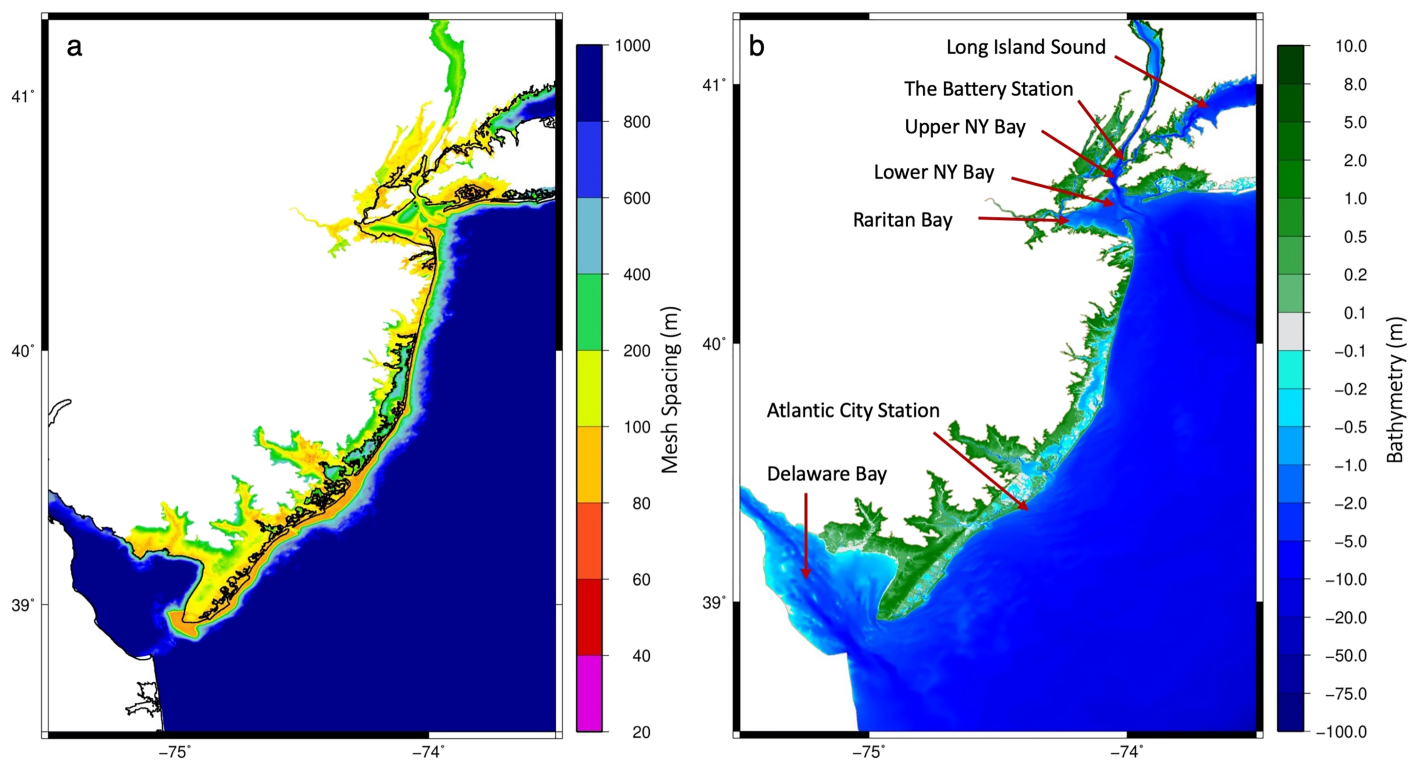


Figure 2. (a) Depiction of the FEMA Region II mesh spacing for the NJ-NY coastal region. (b) Bathymetric heights along the NJ-NY coast. The location of various points of interest are highlighted.

The hourly 10-m winds and surface pressure fields obtained from the HWCM-simulated storms were used as atmospheric forcing to the hydrodynamic and wave models (i.e., one-way coupling between atmospheric and oceanic components). The wind and atmospheric pressure fields were spatially interpolated onto the SWAN+ADCIRC model domain and temporally interpolated to correspond with the SWAN+ADCIRC model time step of 1 s. SWAN+ADCIRC have been tightly coupled to run on the same unstructured grid, and information passes between the two every 10 min without the need for further interpolation (Dietrich et al., 2012; Dietrich, Zijlema, et al., 2011). SWAN is driven by wind speeds, water levels, and currents computed by ADCIRC after the implementation of the atmospheric forcing. The coupled SWAN+ADCIRC model has been tested and validated and has been used extensively in storm surge studies (Akbar et al., 2017; Dietrich et al., 2012; Marsooli & Lin, 2018). While the experimental design prevents the comparison of simulated storm surge to observed water level, both the computational mesh and the coupled model setup have been previously tested (FEMA, 2014a; Ramos-Valle et al., 2018). Moreover, uncertainties in atmospheric forcing are addressed by performing the HWCM ensemble of synthetic tracks.

The bottom friction in the model is parametrized using the quadratic bottom friction law. The Garratt (1977) wind drag formulation was used to calculate the wind drag coefficient with a cap at 0.0035. The density of air was set to the model default at 1.15 kg/m^3 , and the Coriolis parameter was set to vary spatially throughout the domain. For simplicity, and with the purpose of isolating the effect of storm landfall angle on storm surge, tidal forcing was not included in this study. As the synthetic cyclones are not associated with a specified date/time, these would occur at a random stage of a chosen tidal cycle. Additionally, the influence of nonlinear tidal-surge effects, which have been found to be large in the NJ-NY Harbor (NYH) region (Lin et al., 2010), would have had to be considered in the attempt of isolating the effect of landfall angle on storm surge. Tidal effects must be considered for real cases and in the application of the results presented herein.

The storm surge scenarios produced by coupling the HWCM ensemble of synthetic cyclones with the SWAN+ADCIRC modeling system were assessed. The extent of the inland flooding produced by the storms was estimated over the region bounded within latitudes 38.9°N and 41.5°N and longitudes -72.0°W and -75.7°W . The potential inundation area was calculated by inspecting the dry nodes in the mesh, within

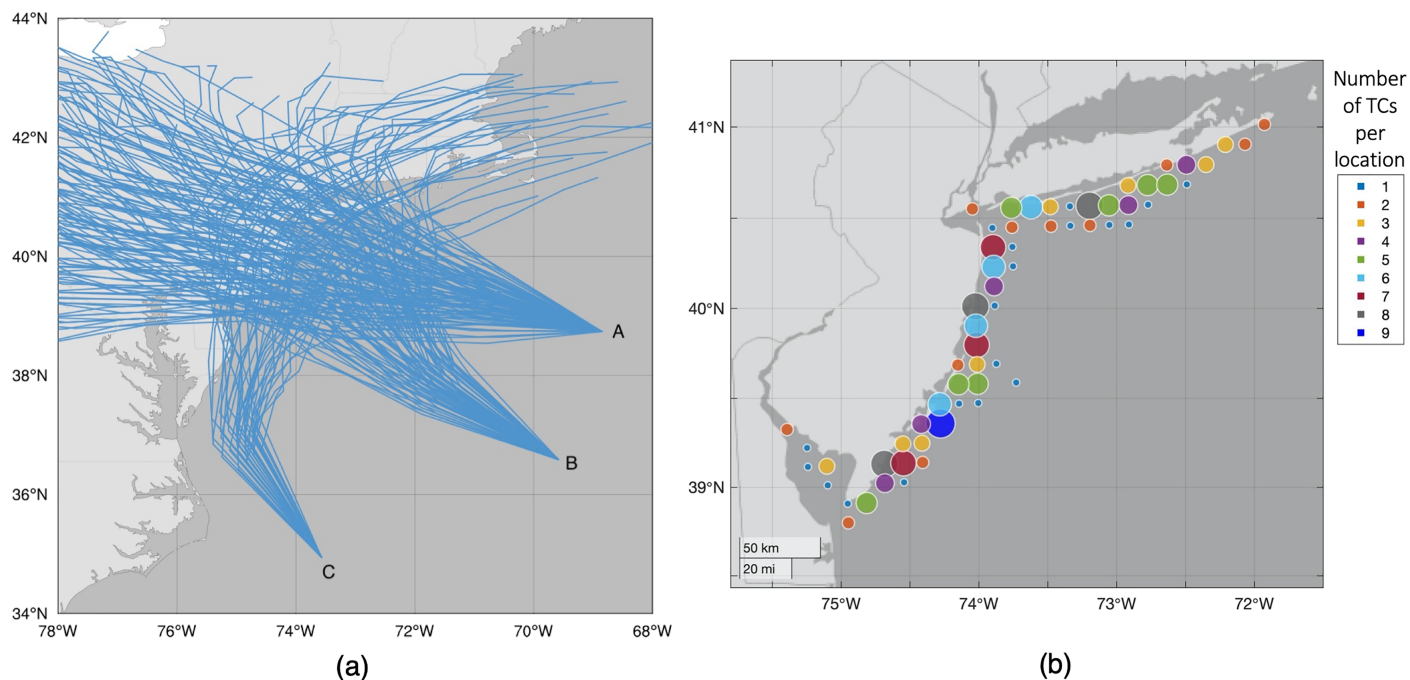


Figure 3. (a) Synthetic cyclone tracks for the 198 TCs resulting from the HWCM ensemble. Synthetic cyclone tracks are shown at 6-hr intervals for 60 hr after cyclone placement in the real-world domain. (b) The landfall location density map.

the specified bound, prior to the start of the simulation. Elements with more than two nodes inundated at any point throughout the simulation were accounted for in the estimate of the inundation area. The estimates for inundation volume were calculated by multiplying the average maximum water elevation within each element by the area of the element. The volume estimates can then be interpreted as a volume potential.

3. Results

3.1. Evaluation of Simulated Synthetic Tracks

The method presented relied on the effective implementation of the HWCM model in simulating synthetic storms. Although an extensive validation of the HWCM is beyond the scope of this paper, we evaluated the use of this methodology by assessing whether the behavior of the synthetic tracks was a response of model internal variability or if it was in fact a response to the external forcing imposed.

Figure S1 in the supporting information shows the resulting tracks from the test case for two HWCM synthetic storms. Details of the simulations are provided in the supporting information (Text S1). The cyclones are subjected to the effect of the model internal variability due to the nonlinear nature of the system. However, the behavior observed from the synthetic tracks is indicative of a response that is mainly due to the external forcing imposed at the lateral boundaries, which dominates the overall movement and behavior of the cyclones. We used this feature to create an ensemble of storms that provide the desired spread in landfall locations and impact angle, which would have not been generated by solely exploiting the internal variability of the model.

3.2. HWCM+ADCIRC Ensemble

We performed more than 300 simulations using the HWCM during the testing phase of the model configuration. A total of 198 simulated tracks were chosen as a subset to create the ensemble of synthetic tracks (shown in Figure 3a). The tracks selected included those cyclones that made landfall at any point along the NJ-NY coastline. Even though an equal number of simulations were tested for each of the three initial storm locations, the resulting ensemble produced fewer number of landfalling synthetic tracks originating from the southernmost point (Point C in Table 1). These tracks are categorized as parallel-moving tracks

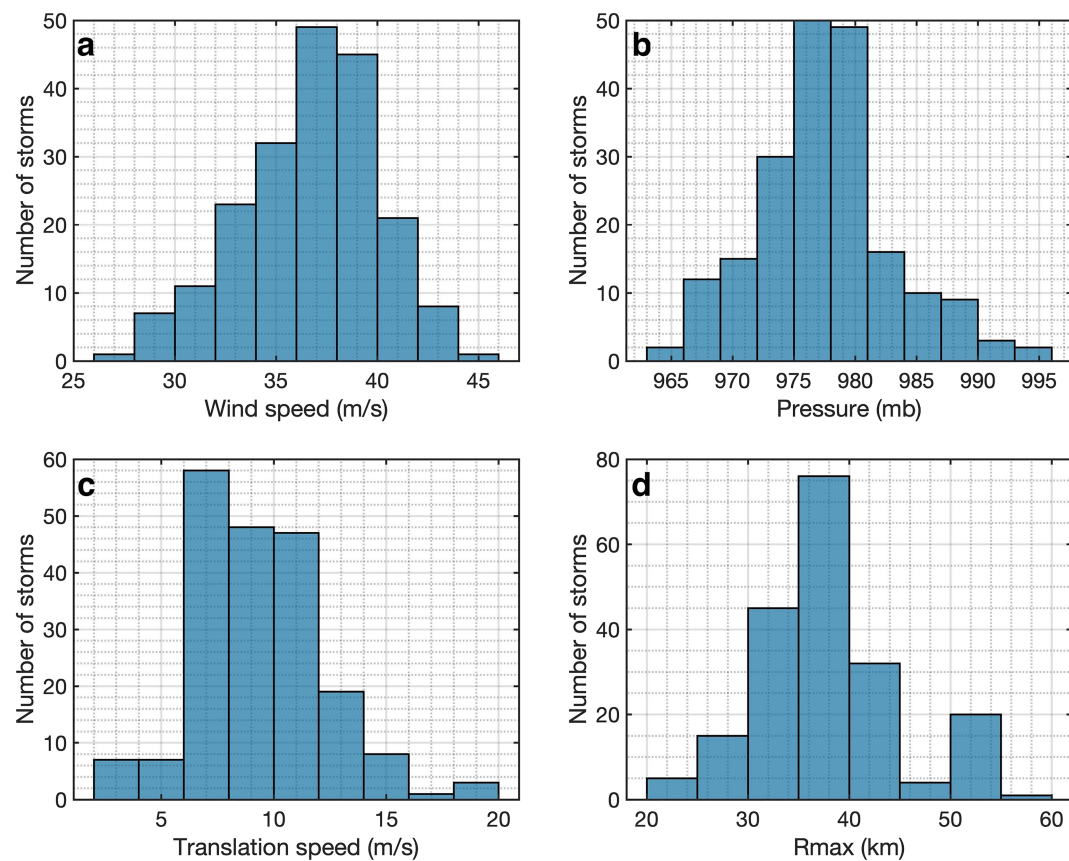


Figure 4. Distribution of (a) wind speed (m/s), (b) minimum pressure (mb), (c) translation speed (m/s), and (d) radius of maximum winds (km) for the 198 HWCM simulated synthetic cyclones.

relative to the NJ coast and have been known historically to be more common than tracks moving from offshore at more slanted angles. The combination of TC initial location and background wind flow resulted in fewer parallel landfalling cyclones. The simulation resulted in 97 tracks originating from point A, 73 from point B, and 28 from point C.

The density map in Figure 3b shows the extent and ample coverage of the ensemble members along the entire NJ-NY coastline. The average distance between adjacent landfall points is 12 km.

The distribution of storm parameters (Figure 4) were examined and compared to the historical record. Henceforth, we identify each track by the maximum wind speed, minimum pressure, radius of maximum wind (R_{\max}), and translation speed at the time step prior to landfall.

The range of TC intensities, as given by the maximum wind speed at landfall, varies from 26 to 46 m/s (i.e., tropical storm to Category 2 intensity). About 85% of the cases in the ensemble fall within the range of 33–42 m/s (i.e., Category 1). Generally, the intensity of TCs that make landfall in the U.S. North Atlantic Coast is rarely higher than that of a Category 1 storm (Marsooli & Lin, 2018). Even though the initial vortices inserted in the real-world domain ranged from Category 2 to 4 intensity, the environment did not sustain these intensities throughout the storm's lifetime and by landfall the storms had weakened to mostly Category 1 cyclones. This is an expected outcome since in addition to weakening at landfall, the TCs weaken as they stabilize after being transposed to the real-world domain. The ensemble distribution of maximum wind speed falls within the probability density function of maximum intensity at landfall for North Atlantic TCs, which peaks at around 43 m/s (Landsea et al., 2015).

The range of translation speed in the probability density function for North Atlantic TCs (1989–2000) varies from 0 to 18 m/s with a peak between 4 and 6 m/s (Kaplan & DeMaria, 2003). The translation speed for the HWCM ensemble members is consistent with the North Atlantic TC record as storm motion ranges between

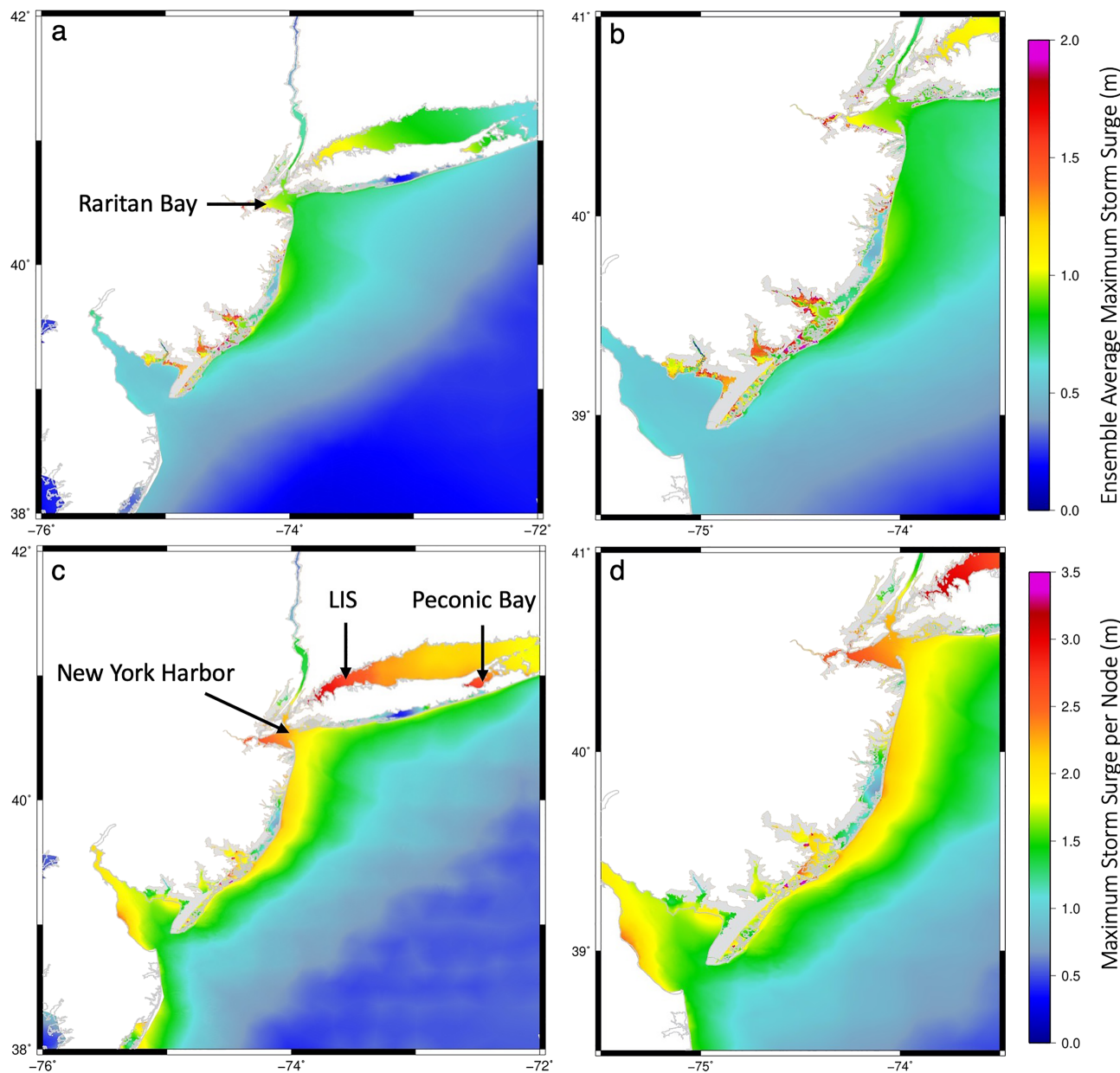


Figure 5. (a) Ensemble average of maximum water level. (b) Zoom in of (a) along the New Jersey coast. (c) Maximum water elevation forecasted at each node. (d) Zoom in of (c) along the New Jersey coast.

3 and 19 m/s, with a similar peak in the distribution between 6 and 8 m/s. The mean R_{\max} of Atlantic Basin TCs from 1988 to 2008 is estimated to be around 64 km with a standard deviation of 39.6 km (Quiring et al., 2011). The radius of maximum winds for the HWCM ensemble has a narrower range in the distribution (20–60 km) and is generally characterized by smaller TCs, with the majority of the storms having an R_{\max} within the range 30–40 km.

The ensemble average maximum storm surge (Figures 5a and 5b) is above 1.5 m in various locations along the coast including regions of southern NJ and Raritan Bay, highlighting these areas' vulnerability and sensitivity to different types of storms. In this scenario Figures 5c and 5d, where the maximum elevation per node is contoured. In these scenarios, some areas such as the NYH (encompassing the Upper New York Bay, Lower New York Bay, and Raritan Bay), LIS, Peconic Bay, and the inlets along the south coast of NJ experienced a maximum storm surge of over 2.5 m for given cases. These areas

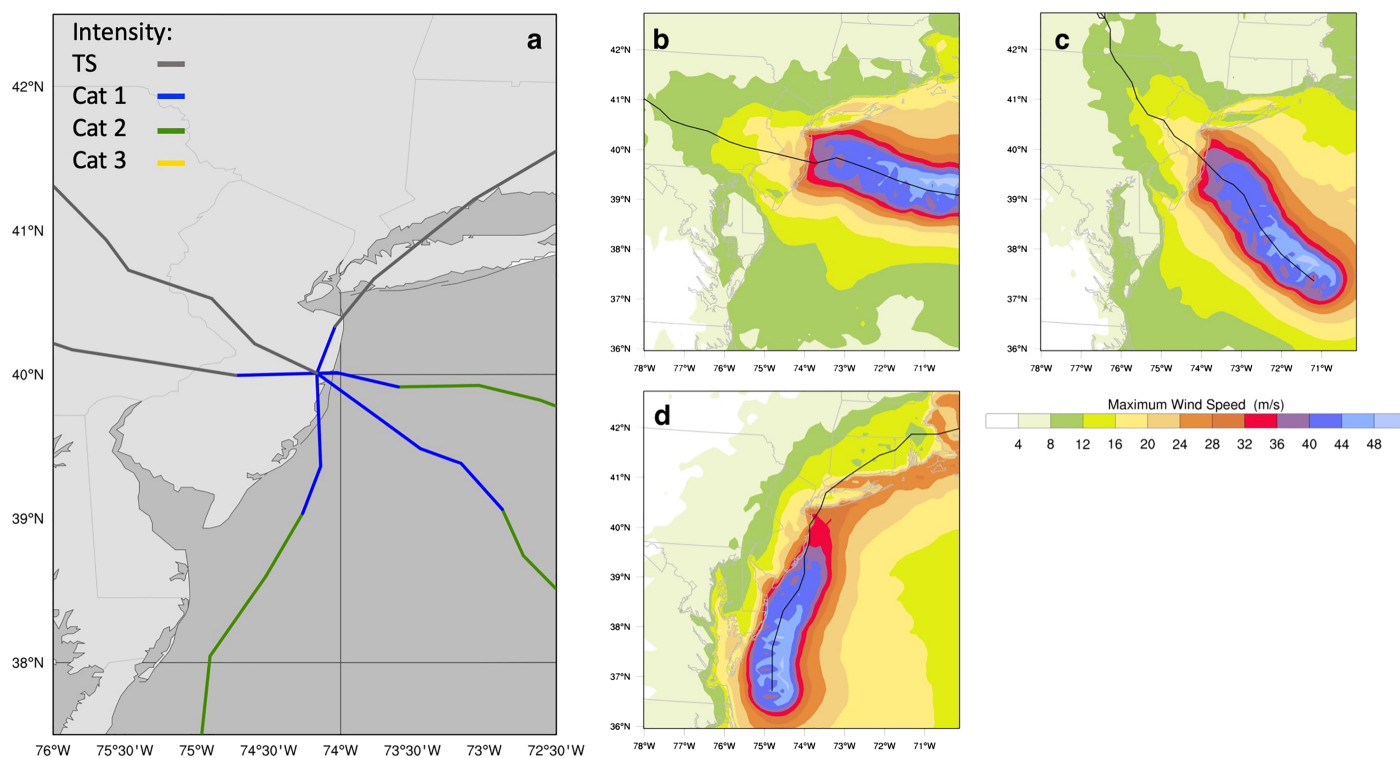


Figure 6. (a) Case study to explore relationships between TC landfall angle and storm surge. Maximum wind speed fields for the (b) perpendicular, (c) diagonal, and (d) parallel cases.

represent high vulnerability regions with an increased likelihood of experiencing substantial storm surge impact.

3.3. The Effect of TC Landfall Angle on Storm Surge

3.3.1. A Case Study Along the Coast of NJ

The density map of landfall locations shown in Figure 3b allowed us to determine sites where multiple TCs made landfall. We examined various cases where cyclones approached the selected landfall locations from various directions. Henceforth, the tracks are categorized according to their general direction with respect to the NJ coast; thus, they are based on the initial storm placement in the real world (i.e., points A–C in Table 1). To isolate the effect of landfall angle and allow for a more direct comparison between the cyclones, we minimized the differences among the TC's physical parameters. The TC selection process began with identifying the tracks that crossed any given location within a 20-km radius centered on a point of reference near the coast. From this initial selection, we only included the TCs that had maximum wind, translational speed, and R_{max} within $\pm 0.5\sigma$ of the mean of all storms crossing the 20-km radius. Various points along the NJ coastline were examined, and similar results were found among these test cases. Only one of the cases is presented here (Figure 6a).

The tracks chosen for this reference point intersect along the coast as they make landfall, approximately 23 hr after the simulation was initialized. From Figures 6b–6d the similarities among the wind field structures are shown. For all three cases, the lifetime maximum wind speed occurred on the right-hand side of the TCs during the first forecast hours of the simulation. The range of maximum wind speed at landfall for the three tracks is narrow, ranging between 34.5 and 35 m/s. The difference with respect to the TC maximum wind speed parameter mean was calculated for each of the tracks per hourly time step. The average difference in maximum wind speed within the first 24 hr was 0.38, 0.43, and -0.81 m/s for the perpendicular, diagonal, and parallel tracks, respectively, while the actual differences fluctuated to ± 3.0 m/s close to landfall time. The estimated difference in maximum wind speeds began to diverge after the storm had made landfall, ensuring similarities between the storms up to that point. Similarities in the TC size are also highlighted

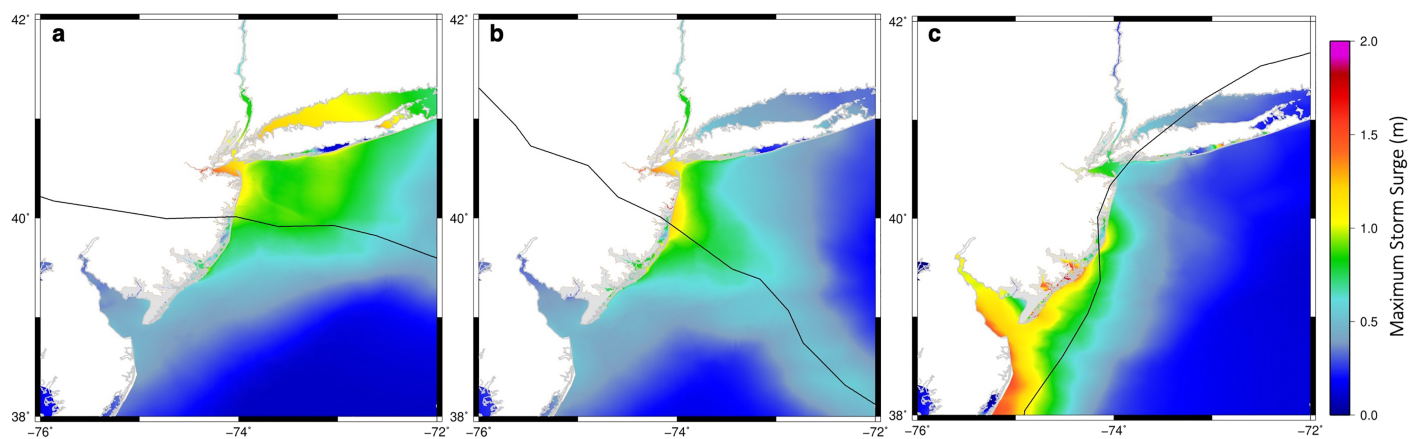


Figure 7. Maximum storm surge levels for the (a) perpendicular, (b) diagonal, and (c) parallel tracks in the case study. Tracks are plotted near landfall at 3-hr intervals.

in Figures 6b–6d. The TCs are characterized by R_{\max} within the range of 33–37 km. The diagonal track has the highest R_{\max} of 37 km, while the perpendicular and parallel tracks both have an R_{\max} estimated at 33 km at landfall. The variation in translation speed is also subtle varying between 6.47, 7.23, and 9.15 m/s for the parallel, perpendicular, and diagonal tracks, respectively.

While the differences among the synthetic cyclone characteristics were minimized, the maximum storm surge patterns in Figure 7 highlights the differences in impact area as well as the differences in offshore surge extent. At the Battery, the peak storm surge ranged from 1.06, 1.09, and 0.72 m for the perpendicular, diagonal and parallel tracks, respectively. Most of the impacts from the parallel track (Figure 7c) were observed in the Delaware Bay and along the southern coast of NJ, coinciding with regions of intense winds. As the storm advanced along the coast, the strongest winds were often directed toward the coast. The parallel case also produced the highest inundation volume, estimated at about 0.6059 km^3 . For the diagonal track in Figure 7b, storm surge heights above 1.0 m are more localized and centered more closely to the landfall location than those for the other two cases. Due to its more oblique angle, as the storm moved toward the coast, the strongest winds in the right-hand side of the TC remained over open ocean for a longer period of time. Closer to landfall, NE winds directed toward the coast caused high storm surge in this area. As the storm continued its movement, easterly winds were directed into the NYH area. The inundation volume for the diagonal case was 0.2153 km^3 . The perpendicular case shows the extent of stronger winds over the LIS and NYH regions, corresponding with the locations where maximum storm surge was generated. As the TC approached land, a shift from N/NE winds to purely easterly winds along the fetch direction over the LIS caused a buildup of water as inferred from Figure 7a. Similarly to the diagonal case, easterly winds are directed toward the NYH region. In both cases, the direction and magnitude of the winds force water into small areas, suggesting a larger potential for inland flooding. While the perpendicular track had a broader offshore impact and extent than had the other two tracks, it had the lowest estimated volume of 0.1574 km^3 .

3.3.2. Ensemble Simulations to Assess the Effect of Cyclone Landfall on Storm Surge

To generalize the conclusions drawn for the case study, we specifically examined the HWCM-simulated tracks that made landfall in NJ and their corresponding average maximum storm surge. The simulated tracks were also classified into the same three storm types, namely, perpendicular, diagonal, and parallel, based on their initial storm placement in the real-world domain (i.e., points A–C respectively in Figure 3a). The filtering resulted in 59 perpendicular, 43 diagonal, and 11 parallel cases (Figures 8a–8c).

The distributions of TC parameters in Figure 9 show the variability and spread among the individual cases in each directional category. These distributions have been normalized by the number of cyclones per directional category to account for the differences in the number of cyclones. With mean wind speeds of 34, 37, and 37.5 m/s for the parallel, diagonal, and perpendicular tracks, respectively, on average, they are all characteristic of a Category 1 TC (Figure 9a). The distributions for translation speed and radius of maximum winds (Figures 9c and 9d) show less variability than the intensity parameters. The peak in the distribution of R_{\max} for each storm type cluster closely to each other and have a large spread. The R_{\max} distribution

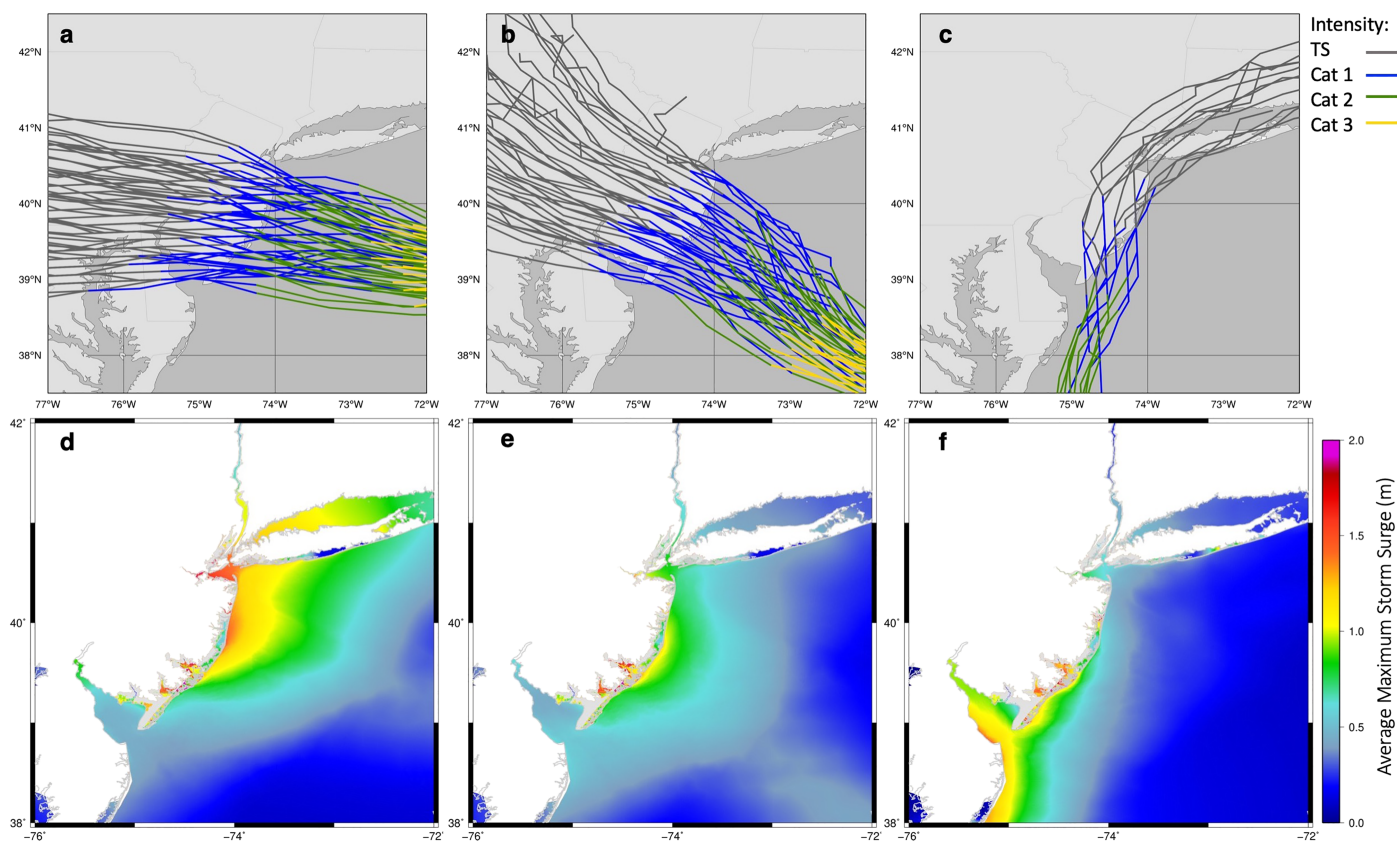


Figure 8. The tracks that made landfall in NJ were considered to investigate the effect of TC landfall angle and location on storm surge. The clustering resulted in (a) 59 perpendicular tracks, (b) 43 diagonal tracks, and (c) 11 parallel tracks with respect to the NJ coast. (d–f) The corresponding maximum storm surge levels, showing the differences in offshore extent.

peaks between 32 and 36 km for the perpendicular and diagonal tracks and between 36 and 40 km for the parallel tracks. The distribution of translation speed shows the tendency of parallel tracks toward slower motions (mean of 7.5 m/s) and the perpendicular tracks toward faster motions (mean of 11.3 m/s).

While the magnitude of the resulting mean maximum storm surge is similar among the three groups, these mostly reflect an impact on the storm surge location and extent, as was previously seen in the case study (Figure 7) in section 3.3.1. On average, the parallel tracks had a larger effect in the Delaware Bay and along the southern NJ coast (Figure 8f). Since all the parallel tracks directly interact with land before reaching the NYH and LIS regions, little impact was seen in these areas from this type of storm. The perpendicular and diagonal tracks in Figures 8d and 8e share some similarities in terms of the location where the highest storm surge was produced. Their difference mostly lies in the offshore extent of storm surge. For the perpendicular cases, the average maximum storm surge resulted in a broader surge extent affecting more areas in NY such as LIS and the NYH region. For the diagonal tracks, the offshore storm surge extent was narrower than the average pattern resulting from the perpendicular tracks.

To assess inland flooding, we examined the inundated area and potential inundation volume. The inundation volume estimates consider both the extent of the area inundated and the magnitude of the flooding. This metric provides a broader assessment of the impact associated with each storm direction. The mean inundation area for the parallel tracks is 469 km^2 , which accounts for about 16% of the potential flooding area ($2,940 \text{ km}^2$). A larger sample of parallel cases would be useful to validate this result. The mechanisms behind this finding are likely due to two factors regarding the storm track itself and the region of impact. First, while the impact of parallel tracks on any specific region along the coast is of shorter duration, parallel tracks affect more of the coastline as they move alongshore and as such have a larger potential for inundation. In addition, the increase in inundation volume is due to the vulnerability of the area near landfall due to its

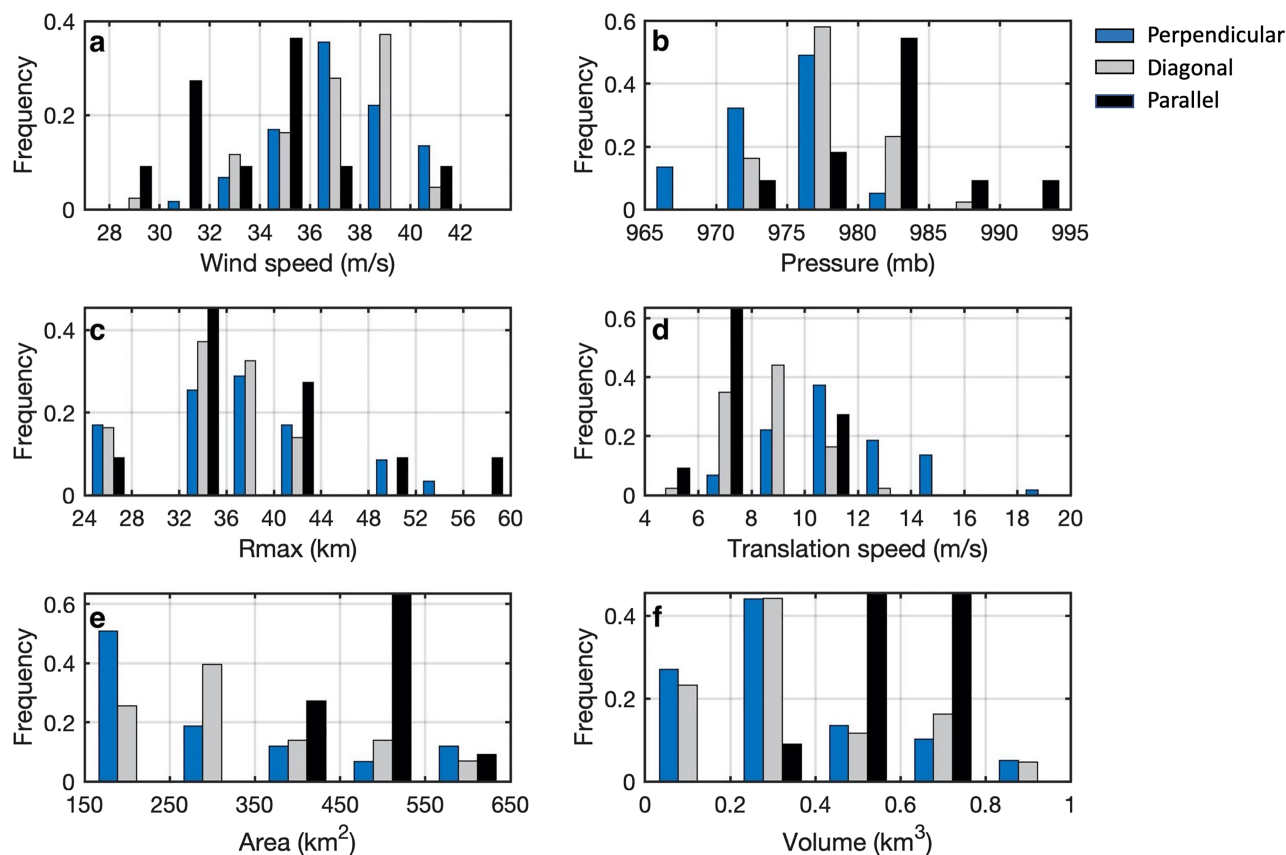


Figure 9. Distribution of (a) wind speed (m/s), (b) minimum pressure (mb), (c) radius of maximum winds (km), (d) translation speed, (e) inundation area (km²), and (f) inundation volume (km³). The distributions are normalized by the number of storms per category.

low-lying topography. We have seen from the maximum water levels in Figure 8 that the region of inlets in southern NJ is particularly vulnerable to storm surge. The perpendicular and diagonal cases exhibited a wider range of inundation scenarios (Figure 9f), with most cases tending to inundate between 150 and 350 km².

The parallel tracks produced the largest mean inundation volume of 0.57 ± 0.10 km³. The mean volume estimates for the perpendicular tracks were lower (0.35 ± 0.22 km³), albeit with a larger variability, than those for the diagonal cases (0.37 ± 0.21 km³). The results for inundation area and volume prove somewhat unexpected and counterintuitive to what the maximum storm surge patterns depict in Figures 8d–8f. While the maximum surge level patterns point to the highest potential for inland flooding for perpendicular tracks, the mean inundation values suggest that these storms produced the least inundation in terms of both the extent and the flood volume. However, the perpendicular cases were actually responsible for the largest inundation area produced by any of the storms in the ensemble.

To address this further, we examined the top 10 surge-producing storms per directional category (Figure 10) and the corresponding inundation volume at two locations: The Battery and Atlantic City stations (National Oceanic and Atmospheric Administration/National Ocean Service/Center for Operational Oceanographic Products and Services, n.d.), chosen to correspond in the model with their actual placement as given by the National Oceanic and Atmospheric Administration Tides and Currents stations. At the Battery (Figure 10b), there is a clear distinction as to the effect of storm landfall angle on storm surge. Perpendicular tracks produced the highest storm surge impact, followed by the diagonal and parallel cases. At Atlantic City (Figure 10a), the sensitivity to landfall angle was not that apparent. While the perpendicular tracks did produce the highest peak storm surge at the Atlantic City station, all three storm types produced substantial and comparable peak surge heights relative to all the storms in the ensemble (between 0.84 and 1.71 m). When examining the top 10 storms producing peak levels at the Battery, the parallel cases caused

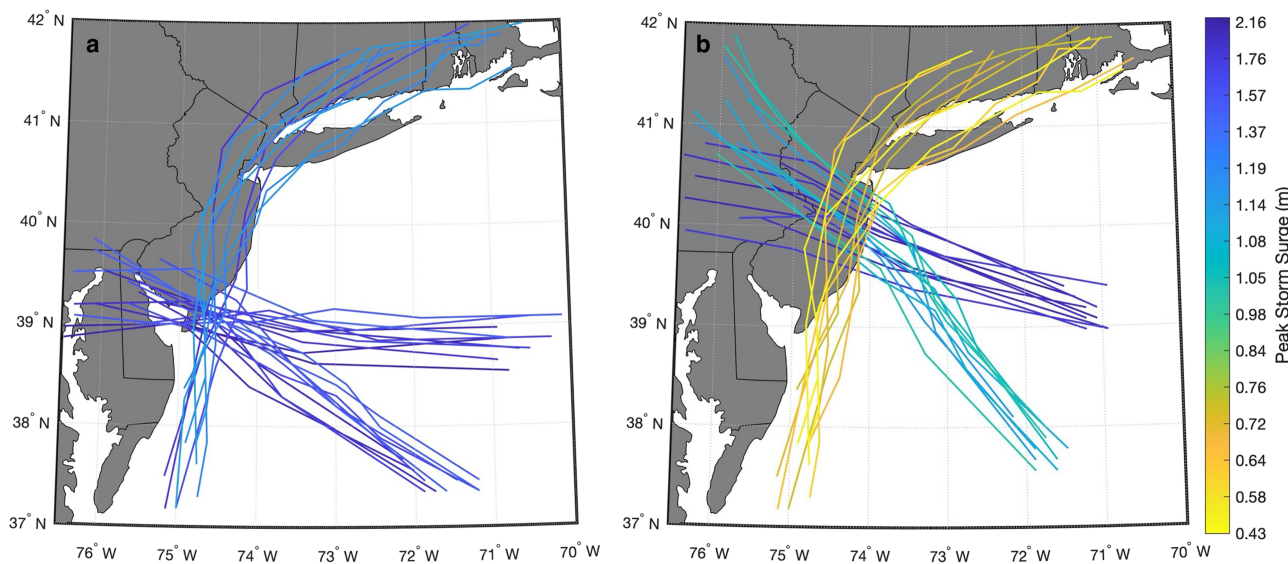


Figure 10. Simplified tracks for the storms that produced the top 10 highest storm surges for each of the categories at (a) Atlantic City and (b) The Battery stations. The tracks are identified based on the magnitude of the peak storm surge.

the lowest peak surge (0.48 m) but still exhibited a tendency to flood a larger volume than its counterparts. For Atlantic City the opposite was observed. Along the south coast of NJ, in the area of highest flooding potential, the perpendicular tracks had the highest flood volume estimates, while the parallel had the lowest. This result points to the relevance of landfall location in the assessment of storm surge sensitivity, which is explored in more detail in section 3.4.

3.4. Clustering by Storm Surge Scenarios

Initially, the HWCM ensemble of simulations were grouped in a subjective manner based on the general direction of the storm track. In this section, we present a different approach by performing a *K*-means clustering on the spatial distribution of maximum storm surge levels rather than clustering by storm track direction. After the clustering, we examined the characteristics of the associated storms classified within each cluster. We were interested in using this tool to objectively examine the link between cyclone landfall angle and location with the resulting storm surge. The clustering was done for the 113 cases that made landfall in NJ. The variance ratio criterion (Caliński & Harabasz, 1974) was employed to determine the optimal number of clusters, which resulted in the use of four clusters (C1–C4).

The storm tracks associated with each cluster are shown in Figure S2 of the supporting information. Two of the main features resulting from the cluster are (i) the fact that two out of the four groups are composed of tracks approaching the coast from different angles and (ii) the distinction between the TCs' landfall locations. Cyclones in clusters C1 and C3 have a similar landfall location along the southern coast of NJ (Figures S2a and S2e), while cyclones in C2 and C4 have an impact further north along the coast (Figures S2c and S2g). We further separated the clusters composed of different track categories such that for C3 we distinguish between C3 (diagonal) and C3 (parallel) and for C2 we distinguish between C2 (perpendicular) and C2 (diagonal) (Table 2). Upon inspection of the maximum storm surge levels for the individual categories, the patterns previously observed in the case study were repeated, as shown in Figures S2b and S2h for perpendicular cases.

Table 2
Range and Mean Values for Physical Parameters That Characterize the Cyclone Within Each Cluster

Measure	Maximum wind speed (m/s)	Minimum pressure (mb)	Translation speed (m/s)	Radius of maximum wind (nm)
C1 (perpendicular)				
Range	35.18–41.46	969.5–979.2	9.71–14.48	13–27
Mean	37.80	974.35	11.95	20.29
C3 (parallel)				
Range	28.97–40.32	972.8–993.4	4.57–10.24	14–32
Mean	34.02	982.45	7.47	21.27
C3 (diagonal)				
Range	34.96–41.26	972.5–980.3	7.24–13.74	13–23
Mean	37.99	976.39	9.06	18.05
C2 (perpendicular)				
Range	31.66–40.42	974.3–980.8	6.47–13.35	14–29
Mean	35.33	977.98	9.65	21.21
C2 (diagonal)				
Range	28.32–39.33	973.7–988.4	4.57–11.67	14–23
Mean	35.81	979.11	8.53	19.48
C4 (perpendicular)				
Range	35.83–42.70	966.8–987.2	6.47–18.87	13–27
Mean	38.89	972.47	12.24	18.57

While the cluster analysis was performed on the spatial distribution of the maximum water level, we were interested in examining how the characteristics of the storms producing such spatial patterns in each cluster are grouped. The characteristics of the synthetic storms that generated the surge patterns in each of the clusters were examined. Table 2 presents the range and mean values for various TC parameters. Notable differences between the clusters and subclusters are not immediately apparent. As shown for the maximum wind speed in Figure 11b, while some clusters (such as C4) tend to have slightly stronger storms, the resulting clusters do not appear to be primarily based on the maximum wind speed or by any of the other physical characteristics inherent to the cyclones. Figure 11d also showed that clusters such as C2 and C3 have slower moving storms than have C1 and C4, which could point to the reason the perpendicular tracks of C2 and C4, with similar landfall location, are not clustered together.

As expected, the results highlight how each of the clusters was classified by various water elevation metrics such as the maximum storm surge estimate of overall inland flooding. Figure 11a shows the distinction of clusters by landfall location, separating the tracks that make landfall further north and south along the NJ coastline. The tracks that make landfall along the southern coast of NJ (C1 and C3) show a larger flooding volume than do the tracks that make landfall along the northern portion of the NJ coast (C2 and C4). The range of inundation volumes for the southern cases was 0.5496–0.6570 km³. For the northern cases, the range was 0.1859 – 0.2636 km³. On average, within each of the northern and southern cases, the perpendicular tracks were responsible for the highest inland flooding potential. Figure 11c highlights the pattern of decreasing flood volume with increasing latitude. The results from the clustering method highlight more directly the sensitivity of storm surge not only to the landfall impact angle but to landfall location.

4. Discussion

The use of the HWCM in simulating synthetic tracks allowed us to control the characteristics of the cyclones, as the tracks responded to the external forcing imposed at the boundaries. This feature in the HWCM, allowed us to generate the desired spread in the ensemble to assess the sensitivity of storm surge to cyclone landfall angle.

We showed that the main difference between the TC directional groups manifested in the location and extent of the storm surge impacts. The parallel cases simulated in this study make landfall in south NJ, and the resulting storm surge mostly impacts the Delaware Bay and southern NJ coast. If we considered parallel storms that moved along the coast without making landfall, we could expect these to have a higher and broader impact than would the parallel cases examined here. These tracks would likely continue their movement along the coast without the decrease in intensity they undergo after landfall. Given that the perpendicular and diagonal tracks do not interact with land prior to their landfall, we were able to compare them more directly. On average, the perpendicular tracks exhibited a more widespread extent of the storm surge signal, while the diagonal tracks were shown to impact a smaller region.

The three storm categories exhibited similarities in terms of the upper limit of the inundation extent and volume. On average, the parallel tracks exhibited the tendency to flood a broader area than did the other two directional categories. Nevertheless, the perpendicular tracks, particularly those making landfall in southern NJ, were responsible for the peak inundation within the domain. This result brought into question the potential influence of the mesh extent into the interpretation of the flooding of each category. However, since the mesh extent follows the 25-ft (7.6 m) elevation contour, it is inherently designed to account for actual potential flooding areas based on the region's topographic features. Thus, the mesh represents the area that can be flooded in reality and does not bias the results presented. Storms impacting the southern NJ area have a higher flooding potential than those in other areas further north along the coast. The dependency of peak storm surge to the landfall angle in southern NJ was lower. Nevertheless, when comparing storms affecting the area of highest flooding potential, we found the perpendicular tracks have a greater effect, inundating a larger volume. More broadly, the flooding potential along the NJ coast was not uniform and decreased with increasing latitude. The storm surge impact from TCs thus varied depending on its landfall location along the coast, pointing to the importance of geographical (e.g., coastal slope and complexity) and topographic features. The importance of these features in amplifying or reducing storm surge have been quantified in previous studies (Bilskie et al., 2014; Bloemendaal et al., 2019). TCs with landfall in areas with

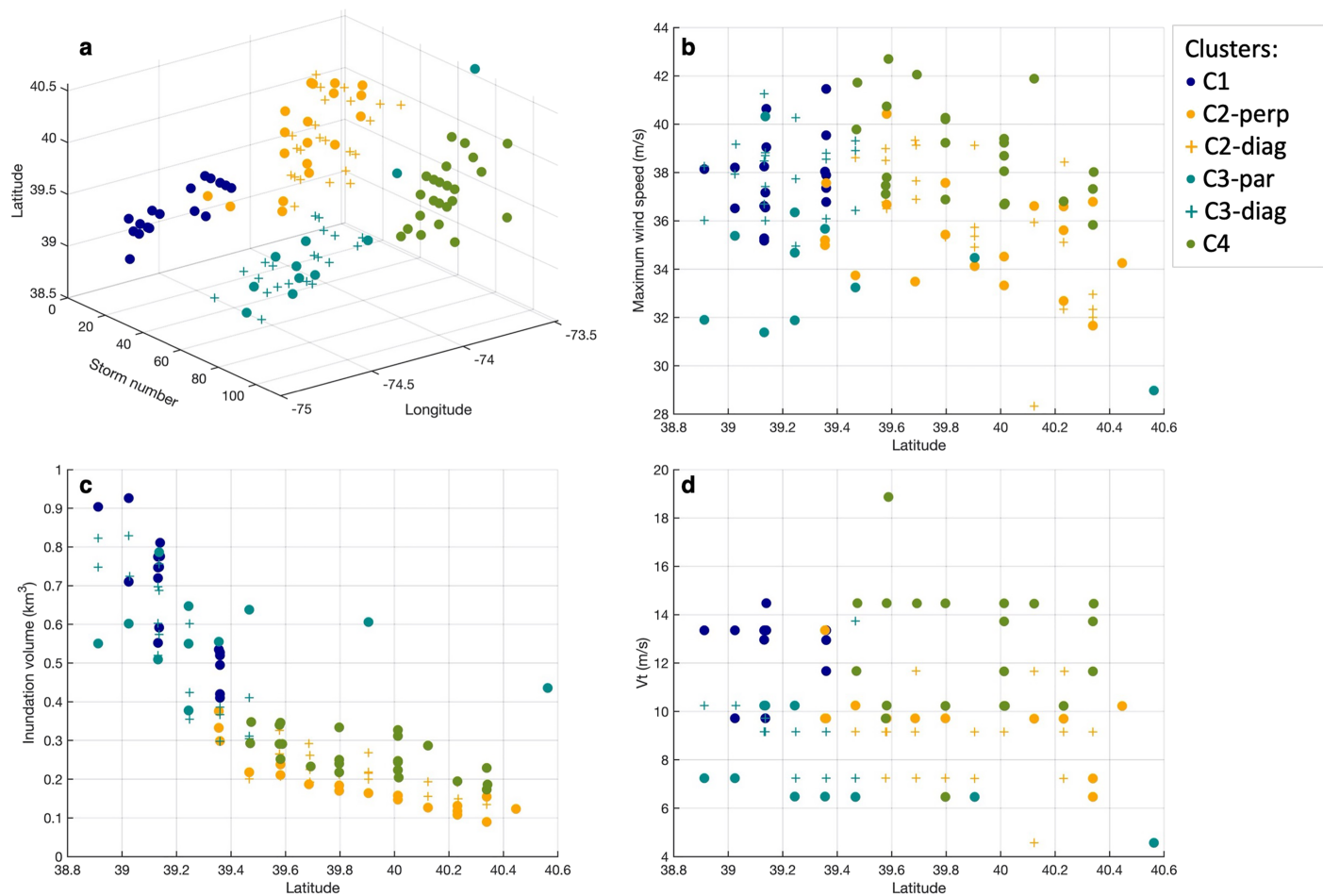


Figure 11. Tropical cyclone and storm surge properties identified by clusters. (a) Landfall location of storms, (b) maximum wind speed at landfall, (c) estimates of inundation volume, and (d) translation speed. TC data in (b)–(d) have been sorted by increasing the latitude coordinate at landfall.

complex coastlines and shallow bathymetry are associated with higher storm surges (Bloemendaal et al., 2019; Mori et al., 2014).

The cluster analysis provided further intuition as to the relationship between landfall angle and location and confirmed the conclusions previously drawn from the HWCM-ADCIRC ensemble. The cluster analysis raised the question of the factors contributing the most to the resulting storm surge. The clusters were not grouped by the TC physical parameters but by the direction of the storms and their general impact location. While it is beyond the scope of this paper, further study is needed to quantify the relative importance of each of the parameters to the resulting storm surge.

The study presented can be enhanced by considering other factors relevant to cyclone-induced inundation and coastal flooding. Results presented here only included the surge and wave components and are thus independent of the tidal cycle and its local effects and of rainfall-runoff contributing to flooding. In reality, the overall inundation volume depends on other factors such as the cyclone-induced precipitation. Rainfall-runoff can contribute to the already high inland flooding, pointing to the importance and need of including this process in storm surge and inundation assessment. While we do not delve into the mechanisms of flooding by both storm surge and rainfall-runoff, it is interesting to note the differences among the cases. Rainfall totals calculated for the cyclones used in the case study (Figure S3 in the supporting information) provide insight into the variations of the precipitation fields and the possible effects of the different storms on the overall flooding. More notable is the parallel case, which showed the highest rainfall totals along the entire coast of NJ and a vast area over Long Island and New York City. The parallel track seemed to have the most potential for inland flooding during the event due to its high precipitation totals along and in close proximity

to the coastline. The perpendicular and diagonal cases might see a delay in the effect on flood heights due to precipitation runoff from distant regions.

TC landfall location and angle play a significant role in modulating storm surge magnitude and inundation. Determining the storm surge sensitivity of the NJ-NY Harbor region to cyclone landfall angle, and generalizing the conclusions to other regions, is complicated due to this dependency and relation to the landfall location of the storms. The methodology presented has the ability of providing further insight into the complex dependencies of storm surge peak heights and inundation volume to landfall angle and impact area while providing a framework applicable to other regions.

5. Concluding Remarks

In this study, we assessed the effect of TC impact angle on the magnitude and extent of storm surge and coastal inundation along the NJ coastline. The use of the HWCM, a recently developed modeling framework based on the WRF model, was implemented to create an ensemble of cyclones approaching the NJ-NY Bight at different angles.

The results of maximum storm surge highlight the difference in surge offshore extent for each of the three directional categories studied. Results indicate a sensitivity to both cyclone approach angle and landfall location. Cyclones with a perpendicular approach angle produce more widespread offshore surge and higher peak surges and have a higher potential for inland flooding, among the categories studied. The level of storm surge sensitivity to landfall angle, however, is not uniform along the coast as some regions were shown to be vulnerable to any type of storm regardless of approach angle (e.g., southern coast of NJ).

While the physical parameters of the storms are relevant, the approach angle and landfall location play a dominant role in the resultant storm surge. These results highlight the need to further quantify the contribution of each parameter to the overall storm surge. Ongoing research focuses on determining the importance of these parameters, at various lead times, in accurately forecasting storm surge.

Acknowledgments

This material is based upon work supported by the National Science Foundation Graduate Research Fellowship Program under Grant DGE-1433187. The authors also acknowledge the support of the National Science Foundation through Award OCE-1419584. Any opinions, findings, and conclusions or recommendations expressed in this material are those of the authors and do not necessarily reflect the views of the National Science Foundation. The authors also acknowledge the National Center for Atmospheric Research, which is a major facility sponsored by the National Science Foundation under Cooperative Agreement 1852977. Model simulations presented in this study are available for download through DesignSafe-CI (at <https://doi.org/10.17603/ds2-9f5y-t459>).

References

- Akbar, M. K., Kanjanda, S., & Musinguzi, A. (2017). Effect of bottom friction, wind drag coefficient, and meteorological forcing in hindcast of Hurricane Rita storm surge using SWAN+ ADCIRC model. *Journal of Marine Science and Engineering*, 5(3), 38. <https://doi.org/10.3390/jmse5030038>
- Bennett, V. C., & Mulligan, R. P. (2017). Evaluation of surface wind fields for prediction of directional ocean wave spectra during Hurricane Sandy. *Coastal Engineering*, 125, 1–15. <https://doi.org/10.1016/j.coastaleng.2017.04.003>
- Bilskie, M., Hagen, S., Medeiros, S., & Passeri, D. (2014). Dynamics of sea level rise and coastal flooding on a changing landscape. *Geophysical Research Letters*, 41, 927–934. <https://doi.org/10.1002/2013GL058759>
- Blake, E. S., Kimberlain, T. B., Berg, R. J., Cangialosi, J. P., & Beven, J. L. II (2013). Tropical cyclone report: Hurricane Sandy. *National Hurricane Center*, 12, 1–10.
- Bloemendaal, N., Muis, S., Haarsma, R. J., Verlaan, M., Irazoqui Apecechea, M., de Moel, H., et al. (2019). Global modeling of tropical cyclone storm surges using high-resolution forecasts. *Climate Dynamics*, 52(7–8), 5031–5044. <https://doi.org/10.1007/s00382-018-4430-x>
- Booij, N., Ris, R. C., & Holthuijsen, L. H. (1999). A third-generation wave model for coastal regions: 1. Model description and validation. *Journal of Geophysical Research*, 104(C4), 7649–7666. <https://doi.org/10.1029/98JC02622>
- Booth, J. F., Rieder, H., & Kushnir, Y. (2016). Comparing hurricane and extratropical storm surge for the Mid-Atlantic and Northeast Coast of the United States for 1979–2013. *Environmental Research Letters*, 11(9), 094004. <https://doi.org/10.1088/1748-9326/11/9/094004>
- Bruyère, C. L., Done, J. M., Jaye, A. B., Holland, G. J., Buckley, B., Henderson, D., et al. (2019). Physically-based landfalling tropical cyclone scenarios in support of risk assessment. *Weather and Climate Extremes*, 26, 100229. <https://doi.org/10.1016/j.wace.2019.100229>
- Calinski, T., & Harabasz, J. (1974). A dendrite method for cluster analysis. *Communications in Statistics—Theory and Methods*, 3(1), 1–27. <https://doi.org/10.1080/03610927408827101>
- Chen, F., & Dudhia, J. (2001). Coupling an advanced land surface-hydrology model with the Penn State-NCAR MM5 modeling system. Part I: Model implementation and sensitivity. *Monthly Weather Review*, 129(4), 569–585. <Go to ISI>://WOS:000168253900001. [https://doi.org/10.1175/1520-0493\(2001\)129<0569:CAALSH>2.0.CO;2](https://doi.org/10.1175/1520-0493(2001)129<0569:CAALSH>2.0.CO;2)
- Cialone, M. A., Grzegorzewski, A. S., Mark, D. J., Bryant, M. A., & Massey, T. C. (2017). Coastal-storm model development and water-level validation for the North Atlantic Coast Comprehensive Study. *Journal of Waterway, Port, Coastal, and Ocean Engineering*, 143(5), 04017031. [https://doi.org/10.1061/\(ASCE\)WW.1943-5460.0000408](https://doi.org/10.1061/(ASCE)WW.1943-5460.0000408)
- Colle, B. A., Bowman, M. J., Roberts, K. J., Bowman, M. H., Flagg, C. N., Kuang, J., et al. (2015). Exploring water level sensitivity for metropolitan New York during Sandy (2012) using ensemble storm surge simulations. *Journal of Marine Science and Engineering*, 3(2), 428–443. <https://doi.org/10.3390/jmse3020428>
- Colle, B. A., Buonaiuto, F., Bowman, M. J., Wilson, R. E., Flood, R., Hunter, R., et al. (2008). New York City's vulnerability to coastal flooding: Storm surge modeling of past cyclones. *Bulletin of the American Meteorological Society*, 89(6), 829–842. <https://doi.org/10.1175/2007BAMS2401.1>
- Dietrich, J., Tanaka, S., Westerink, J., Dawson, C., Luettich, R., Zijlema, M., et al. (2012). Performance of the unstructured-mesh, SWAN +ADCIRC model in computing hurricane waves and surge. *Journal of Scientific Computing*, 52(2), 468–497. <https://doi.org/10.1007/s10915-011-9555-6>

- Dietrich, J., Westerink, J., Kennedy, A., Smith, J., Jensen, R., Zijlema, M., et al. (2011). Hurricane Gustav (2008) waves and storm surge: Hindcast, synoptic analysis, and validation in southern Louisiana. *Monthly Weather Review*, 139(8), 2488–2522. <https://doi.org/10.1175/2011MWR3611.1>
- Dietrich, J., Zijlema, M., Westerink, J., Holthuijsen, L., Dawson, C., Luettich, R. Jr., et al. (2011). Modeling hurricane waves and storm surge using integrally-coupled, scalable computations. *Coastal Engineering*, 58(1), 45–65. <https://doi.org/10.1016/j.coastaleng.2010.08.001>
- Emanuel, K., Ravela, S., Vivant, E., & Risi, C. (2006). A statistical deterministic approach to hurricane risk assessment. *Bulletin of the American Meteorological Society*, 87(3), 299–314. <https://doi.org/10.1175/BAMS-87-3-299>
- Federal Emergency Management Agency. (2011). Redefinition of the coastal flood hazard zones in FEMA Region II: Analysis of the coastal storm surge flood frequencies. In: Federal Emergency Management Agency.
- Federal Emergency Management Agency. (2014a). Region II storm surge project: Mesh development. Washington, DC.
- Federal Emergency Management Agency. (2014b). Region II storm surge project: Model calibration and validation. Washington, DC.
- Fossell, K. R., Ahijevych, D., Morss, R. E., Snyder, C., & Davis, C. (2017). The Practical predictability of storm tide from tropical cyclones in the Gulf of Mexico. *Monthly Weather Review*, 145(12), 5103–5121. <https://doi.org/10.1175/MWR-D-17-0051.1>
- Galarneau, T. J., Davis, C. A., & Shapiro, M. A. (2013). Intensification of Hurricane Sandy (2012) through extratropical warm core seclusion. *Monthly Weather Review*, 141(12), 4296–4321. <https://doi.org/10.1175/MWR-D-13-00181.1>
- Garratt, J. (1977). Review of drag coefficients over oceans and continents. *Monthly Weather Review*, 105(7), 915–929. [https://doi.org/10.1175/1520-0493\(1977\)105<0915:RODCOO>2.0.CO;2](https://doi.org/10.1175/1520-0493(1977)105<0915:RODCOO>2.0.CO;2)
- Gonzalez, V. M., Nadal-Caraballo, N. C., Melby, J. A., & Cialone, M. A. (2019). Quantification of uncertainty in probabilistic storm surge models: Literature review. Retrieved from: <https://apps.dtic.mil/dtic/tr/fulltext/u2/1067548.pdf>
- Hall, T. M., & Sobel, A. H. (2013). On the impact angle of Hurricane Sandy's New Jersey landfall. *Geophysical Research Letters*, 40, 2312–2315. Article. <Go to ISI>://WOS:000328840200076. <https://doi.org/10.1002/grl.50395>
- Holland, G. J. (1980). An analytic model of the wind and pressure profiles in hurricanes. *Monthly Weather Review*, 108(8), 1212–1218. [https://doi.org/10.1175/1520-0493\(1980\)108<1212:AAMOTW>2.0.CO;2](https://doi.org/10.1175/1520-0493(1980)108<1212:AAMOTW>2.0.CO;2)
- Hong, S.-Y., & Lim, J.-O. J. (2006). The WRF single-moment 6-class microphysics scheme (WSM6). *Journal of the Korean Meteorological Society*, 42(2), 129–151.
- Hong, S.-Y., Noh, Y., & Dudhia, J. (2006). A new vertical diffusion package with an explicit treatment of entrainment processes. *Monthly Weather Review*, 134(9), 2318–2341. <https://doi.org/10.1175/MWR3199.1>
- Hussain, M. A., Tajima, Y., Hossain, M. A., & Das, P. (2017). Impact of cyclone track features and tidal phase shift upon surge characteristics in the Bay of Bengal along the Bangladesh Coast. *Journal of Marine Science and Engineering*, 5(4), 52. <http://www.mdpi.com/2077-1312/5/4/52>. <https://doi.org/10.3390/jmse5040052>
- Iacono, M. J., Delamere, J. S., Mlawer, E. J., Shepherd, M. W., Clough, S. A., & Collins, W. D. (2008). Radiative forcing by long-lived greenhouse gases: Calculations with the AER radiative transfer models. *Journal of Geophysical Research*, 113, D13103. <https://doi.org/10.1029/2008JD009944>
- Irish, J. L., Resio, D. T., & Ratcliff, J. J. (2008). The influence of storm size on hurricane surge. *Journal of Physical Oceanography*, 38(9), 2003–2013. Article. <https://doi.org/10.1175/2008JPO3727.1>
- Jelesnianski, C. P., Chen, J., & Shaffer, W. A. (1992). SLOSH: Sea, lake, and overland surges from hurricanes.
- Kalnay, E., Kanamitsu, M., Kistler, R., Collins, W., Deaven, D., Gandin, L., et al. (1996). The NCEP/NCAR 40-year reanalysis project. *Bulletin of the American Meteorological Society*, 77(3), 437–471. [https://doi.org/10.1175/1520-0477\(1996\)077<0437:TNYRP>2.0.CO;2](https://doi.org/10.1175/1520-0477(1996)077<0437:TNYRP>2.0.CO;2)
- Kaplan, J., & DeMaria, M. (2003). Large-scale characteristics of rapidly intensifying tropical cyclones in the North Atlantic Basin. *Weather and Forecasting*, 18(6), 1093–1108. [https://doi.org/10.1175/1520-0434\(2003\)018<1093:LCORIT>2.0.CO;2](https://doi.org/10.1175/1520-0434(2003)018<1093:LCORIT>2.0.CO;2)
- Kimball, S. K. (2008). Structure and evolution of rainfall in numerically simulated landfalling hurricanes. *Monthly Weather Review*, 136(10), 3822–3847. <https://doi.org/10.1175/2008MWR2304.1>
- Kohno, N., Dube, S. K., Entel, M., Fakhruddin, S. H., Greenslade, D., Leroux, M. D., et al. (2018). Recent progress in storm surge forecasting. *Tropical Cyclone Research and Review*, 7(2), 128–139. <https://doi.org/10.6057/2018TCRR02.04>
- Lakshmi, D. D., Murty, P., Bhaskaran, P. K., Sahoo, B., Kumar, T. S., Shenoi, S., & Srikant, A. (2017). Performance of WRF-ARW winds on computed storm surge using hydrodynamic model for Phailin and Hudhud cyclones. *Ocean Engineering*, 131, 135–148. <https://doi.org/10.1016/j.oceaneng.2017.01.005>
- Landsea, C., Franklin, J., & Beven, J. (2015). The revised Atlantic hurricane database (HURDAT2). United States National Oceanic and Atmospheric Administration's National Weather Service. [Available at <http://www.nhc.noaa.gov/data/hurdat/hurdat2-format-atlantic.pdf>].
- Li, Y., Cheung, K. K., & Chan, J. C. (2015). Modelling the effects of land-sea contrast on tropical cyclone precipitation under environmental vertical wind shear. *Quarterly Journal of the Royal Meteorological Society*, 141(687), 396–412. <https://doi.org/10.1002/qj.2359>
- Lin, N., & Chavas, D. (2012). On hurricane parametric wind and applications in storm surge modeling. *Journal of Geophysical Research*, 117, D09120. <https://doi.org/10.1029/2011JD017126>
- Lin, N., Emanuel, K., Oppenheimer, M., & Vanmarcke, E. (2012). Physically based assessment of hurricane surge threat under climate change. *Nature Climate Change*, 2(6), 462–467. Article. <https://doi.org/10.1038/nclimate1389>
- Lin, N., Emanuel, K. A., Smith, J., & Vanmarcke, E. (2010). Risk assessment of hurricane storm surge for New York City. *Journal of Geophysical Research*, 115, D18121. <https://doi.org/10.1029/2009JD013630>
- Lin, N., Marsooli, R., & Colle, B. A. (2019). Storm surge return levels induced by mid-to-late-twenty-first-century extratropical cyclones in the Northeastern United States. *Climatic Change*, 154(1–2), 143–158. <https://doi.org/10.1007/s10584-019-02431-8>
- Luettich, R., & Westerink, J. (2004). Formulation and numerical implementation of the 2D/3D ADCIRC finite element model version 44. XX. Retrieved from Chapel Hill, NC: http://www.unc.edu/ims/adcirc/adcirc_theory_2004_12_08.pdf
- Luettich, R. A., Westerink, J. J., & Scheffner, N. W. (1992). ADCIRC: An advanced three-dimensional circulation model for shelves, coasts, and estuaries. Report 1. Theory and methodology of ADCIRC-2DDI and ADCIRC-3DL. In Dredging Research Program Technical Report DRP-92-6 (pp. 137). Vicksburg, MS: Coastal Engineering Research Center.
- Marsooli, R., & Lin, N. (2018). Numerical modeling of historical storm tides and waves and their interactions along the US East and Gulf Coasts. *Journal of Geophysical Research: Oceans*, 123(5), 3844–3874. <https://doi.org/10.1029/2017JC013434>
- Mayo, T., & Lin, N. (2019). The effect of the surface wind field representation in the operational storm surge model of the National Hurricane Center. *Atmosphere*, 10(4), 193. <http://www.mdpi.com/2073-4433/10/4/193>. <https://doi.org/10.3390/atmos10040193>
- Mori, N., Kato, M., Kim, S., Mase, H., Shibusaki, Y., Takemi, T., et al. (2014). Local amplification of storm surge by Super Typhoon Haiyan in Leyte Gulf. *Geophysical Research Letters*, 41, 5106–5113. <https://doi.org/10.1002/2014GL060689>

- National Oceanic and Atmospheric Administration/National Ocean Service/Center for Operational Oceanographic Products and Services. (n.d.). Tides and currents. Retrieved from <https://tidesandcurrents.noaa.gov>
- Needham, H. F., Keim, B. D., & Sathiaraj, D. (2015). A review of tropical cyclone-generated storm surges: Global data sources, observations, and impacts. *Reviews of Geophysics*, 53, 545–591. <https://doi.org/10.1002/2014RG000477>
- Orton, P., Vinogradov, S., Georgas, N., Blumberg, A., Lin, N., Gornitz, V., et al. (2015). New York City panel on climate change 2015 report chapter 4: Dynamic coastal flood modeling. *Annals of the New York Academy of Sciences*, 1336(1), 56–66. <https://doi.org/10.1111/nyas.12589>
- Peckham, S. E., Smirnova, T. G., Benjamin, S. G., Brown, J. M., & Kenyon, J. S. (2016). Implementation of a digital filter initialization in the WRF model and its application in the Rapid Refresh. *Monthly Weather Review*, 144(1), 99–106. <https://doi.org/10.1175/MWR-D-15-0219.1>
- Quiring, S., Schumacher, A., Labosier, C., & Zhu, L. (2011). Variations in mean annual tropical cyclone size in the Atlantic. *Journal of Geophysical Research*, 116, D09114. <https://doi.org/10.1029/2010JD015011>
- Ramos-Valle, A. (2019). Effect of tropical cyclone landfall angle on storm surge. DesignSafe-CI. <https://doi.org/10.17603/ds2-9f5y-t459>
- Ramos-Valle, A., Curchitser, E., Bruyère, C., & Fossell, K. (2018). Simulating storm surge impacts with a coupled atmosphere-inundation model with varying meteorological forcing. *Journal of Marine Science and Engineering*, 6(2), 35. <http://www.mdpi.com/2077-1312/6/2/35>. <https://doi.org/10.3390/jmse6020035>
- Rego, J. L., & Li, C. (2009). On the importance of the forward speed of hurricanes in storm surge forecasting: A numerical study. *Geophysical Research Letters*, 36, L07609. <https://doi.org/10.1029/2008GL036953>
- Rotunno, R., Chen, Y., Wang, W., Davis, C., Dudhia, J., & Holland, G. (2009). Large-eddy simulation of an idealized tropical cyclone. *Bulletin of the American Meteorological Society*, 90(12), 1783–1788. <https://doi.org/10.1175/2009BAMS2884.1>
- Rotunno, R., & Emanuel, K. A. (1987). An air-sea interaction theory for tropical cyclones. Part II: Evolutionary study using a nonhydrostatic axisymmetric numerical model. *Journal of the Atmospheric Sciences*, 44(3), 542–561. [https://doi.org/10.1175/1520-0469\(1987\)044<0542:AAITFT>2.0.CO;2](https://doi.org/10.1175/1520-0469(1987)044<0542:AAITFT>2.0.CO;2)
- Skamarock, W., Klemp, J., Dudhia, J., Gill, D., Barker, D., Duda, M., et al. (2008). A description of the Advanced Research WRF version 3, NCAR technical note, Mesoscale and Microscale Meteorology Division. National Center for Atmospheric Research, Boulder, Colorado, USA.
- Smith, A. B., & Katz, R. W. (2013). US billion-dollar weather and climate disasters: Data sources, trends, accuracy and biases|SpringerLink. *Natural Hazards*, 67(2), 387–410. <https://doi.org/10.1007/s11069-013-0566-5>
- Thomas, A., Dietrich, J., Asher, T., Bell, M., Blanton, B., Copeland, J., et al. (2019). Influence of storm timing and forward speed on tides and storm surge during Hurricane Matthew. *Ocean Modelling*, 137, 1–19. <http://www.sciencedirect.com/science/article/pii/S1463500318302609>. <https://doi.org/10.1016/j.ocemod.2019.03.004>
- Tiedtke, M. (1989). A comprehensive mass flux scheme for cumulus parameterization in large-scale models. *Monthly Weather Review*, 117(8), 1779–1800. [https://doi.org/10.1175/1520-0493\(1989\)117<1779:ACMFSF>2.0.CO;2](https://doi.org/10.1175/1520-0493(1989)117<1779:ACMFSF>2.0.CO;2)
- Torres, M. J., Reza Hashemi, M., Hayward, S., Spaulding, M., Ginis, I., & Grilli, S. T. (2018). Role of hurricane wind models in accurate simulation of storm surge and waves. *Journal of Waterway, Port, Coastal, and Ocean Engineering*, 145(1), 04018039. [https://doi.org/10.1061/\(asce\)ww.1943-5460.0000496](https://doi.org/10.1061/(asce)ww.1943-5460.0000496)
- Weisberg, R. H., & Zheng, L. (2006). Hurricane storm surge simulations for Tampa Bay. *Estuaries and Coasts*, 29(6), 899–913. <https://doi.org/10.1007/BF02798649>
- Yin, J., Lin, N., & Yu, D. P. (2016). Coupled modeling of storm surge and coastal inundation: A case study in New York City during Hurricane Sandy. *Water Resources Research*, 52, 8685–8699. <Go to ISI>://WOS:000393318600017. <https://doi.org/10.1002/2016WR019102>